ISSN 1063-7834, Physics of the Solid State, 2009, Vol. 51, No. 1, pp. 99–105. © Pleiades Publishing, Ltd., 2009.
Original Russian Text © T.S. Orlova, J.Y. Laval, Ph. Monod, V.S. Zakhvalinskiĭ, V.M. Egorov, Yu.P. Stepanov, 2009, published in Fizika Tverdogo Tela, 2009, Vol. 51, No. 1, pp. 91–97.

MAGNETISM AND FERROELECTRICITY

Effect of Copper Doping on Charge Ordering in $La_{1/3}Ca_{2/3}Mn_{1-y}Cu_yO_3$ ($0 \le y \le 0.07$)

T. S. Orlova[a], J. Y. Laval[b], Ph. Monod[b], V. S. Zakhvalinskiĭ[c], V. M. Egorov[a], and Yu. P. Stepanov[a]

[a] *Ioffe Physicotechnical Institute, Russian Academy of Sciences, Politekhnicheskaya ul. 26, St. Petersburg, 194021 Russia*
e-mail: orlova.t@mail.ioffe.ru

[b] *Laboratoire de Physique du Solide, CNRS ESPCI, Paris, 75231 France*

[c] *Belgorod State University, ul. Pobedy 85, Belgorod, 308015 Russia*

Received March 24, 2008

Abstract—The effect of copper doping on charge-orbital ordering in $La_{1/3}Ca_{2/3}Mn_{1-y}Cu_yO_3$ ($0 \le y \le 0.07$) is studied by measuring the temperature dependences of the magnetization, the electrical resistivity, and the heat capacity in combination with an electron microscopic investigation of the structure. It is demonstrated that copper doping leads to a lowering of the charge ordering temperature T_{CO} and that this decrease is proportional to the decrease in the Mn^{3+} ion concentration. In the temperature range 5–300 K, the semiconducting pattern of the electrical resistivity persists for all values of $0 \le y \le 0.07$. Electron microscope studies have shown that the presence of copper suppresses the formation of a regular superstructure, which is characteristic of the undoped starting compound, beginning already from low concentrations ($y = 0.01$). Differential scanning calorimetry revealed a substantial decrease in the transition entropy at the onset of charge ordering in copper-doped samples as compared to the starting compound. Doping with copper destroys long-range charge-orbital ordering and retains apparently only short-range order.

PACS numbers: 75.47.Lx, 68.37.Lp

DOI: 10.1134/S1063783409010120

1. INTRODUCTION

Numerous publications have been devoted in the recent decade to manganites of the type $R_{1-x}A_xMnO_3$ (where R stands for a rare-earth element, and A, for a divalent cation) exhibiting colossal magnetoresistance [1–5]. With the concentration x of element A varied within a broad range of $0 \le x \le 1$, the system undergoes a series of phase transitions involving different types of ordering, namely, magnetic, structural, and electronic. The ground state of the $La_{1-x}Ca_xMnO_3$ (LCMO) system at the edges of the phase diagram ($x = 0$ and 1) is the state of the antiferromagnetic (AF) insulator, the ferromagnetic (FM) metal for $0.15 < x < 0.50$, and the charge-ordered antiferromagnet for $\bar{x} > 0.50$.

It is presently generally believed that the phenomenon of colossal magnetoresistance is actually the result of an interplay among the crystal phases with different electronic, magnetic, and structural orders; this competition can be strong enough to initiate phase separation [6, 7] between the states of metallic FM and charge-ordered insulator with AF ordering.

Ferromagnetism and charge ordering (CO) are mutually excluding phenomena in the $R_{1-x}A_xMnO_3$ manganites. Ferromagnetism requires delocalization of the e_g electron from Mn^{3+} and its transfer to Mn^{4+} along the Mn^{3+}–O–Mn^{4+} network by the double exchange mechanism [8]. By contrast, charge ordering becomes realized through localization of the e_g electron and of the hole at Mn^{3+} and Mn^{4+}, accordingly, accompanied by certain ordering of these ions [9], which brings about AF order below the Néel temperature T_N.

An intense study was carried out of LCMO compounds with $x < 0.5$ with the FM ground state, whereas the other part of the phase diagram ($x > 0.5$) with the AF CO ground state remained only poorly explored. The origin itself of the charge- and orbitally-ordered phases is still a subject of discussion [10, 11]. CO is traditionally considered as ordering of the Mn^{3+} and Mn^{4+} ions [7]. This charge ordering is believed to be intimately connected with orbital ordering (OO) caused by Jahn–Teller distortion, with the $d(z^2)(Mn^{3+})$ orbitals being oriented perpendicular to the c axis to form a series of oriented chains in the (a–b) basal plane. Lattice distortion is well seen with a transmission electron microscope (TEM). Striped superstructure in the $La_{1-x}Ca_xMnO_3$ system was visualized by TEM for x = 1/2, 2/3, and 3/4 [12, 13]. Some experiments [14, 15] suggested, however, that charge disproportionation between the manganese ions should be substantially less than unity.

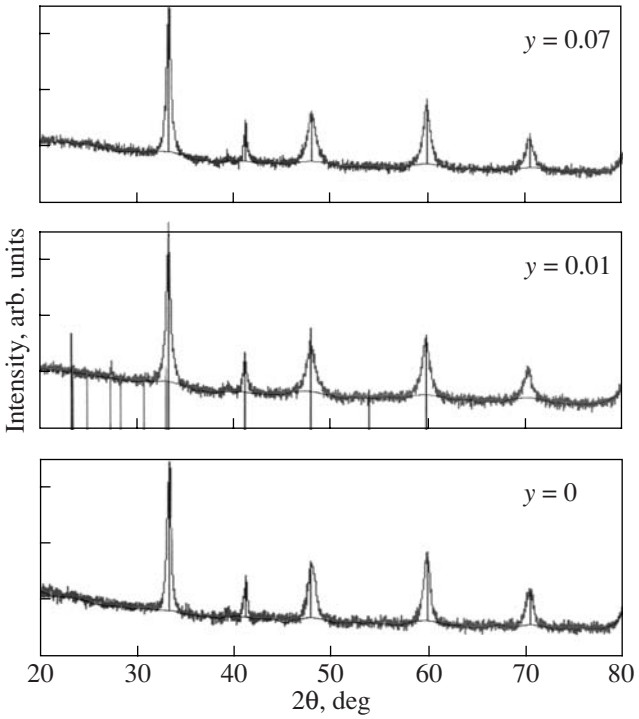

Fig. 1. X-ray diffraction patterns for $La_{1/3}Ca_{2/3}Mn_{1-y}Cu_yO_3$ samples with $y = 0$, 0.01, and 0.07.

For instance, resonant scattering of a synchrotron X-ray beam provided supportive evidence for the existence in $Nd_{0.5}Sr_{0.5}MnO_3$ of manganese of two types, with local lattice distortion, just as expected, having been observed around one of them [14]. The difference in charge between the two configurations was, however, found to be equal approximately to 0.16 electron only, which is far from the one-electron difference accepted in the Mn^{3+} and Mn^{4+} ionic model.

Doping into manganese sites can change substantially the properties of manganites, because this process affects the Mn^{3+}–O–Mn^{4+} bonds. Such doping is considered to be a most efficient method of studying charge and orbital ordering in manganites [16].

Charge ordering phenomena were studied primarily on compositions bordering on the FM and AF ground states in the phase diagrams. Among them are $La_{0.5}Ca_{0.5}MnO_3$ for the LCMO and $Pr_{0.5}Sr_{0.5}MnO_3$ for the PSMO systems. These boundary systems are, however, very sensitive to oxygen content, so that even its slight variation or a small change in the La/Ca or Pr/Sr cation ratio may bring about a shift along the phase diagram, thus transferring the system from the FM to the AF state, or vice versa. Moreover, a characteristic feature of such boundary compositions is phase separation, i.e., the presence of a sizable fraction of FM clusters in the AF host phase, which complicates noticeably investigation of charge ordering in its pure form. This is why we chose for our studies the $La_{1-x}Ca_xMnO_3$ system with $x = 2/3$, in which phase separation was shown [17, 18] to be weak in extent and not to play a prominent part altogether; indeed, at temperatures below that of charge ordering T_{CO} the FM phase occupies less than 0.3% of the total AF host matrix volume [18].

The effect of doping with iron on the charge ordering in $La_{1/3}Ca_{2/3}Mn_{1-y}Fe_yO_3$ ($0 \le y \le 0.06$) was studied in [18]. It was shown that both the charge ordering temperature T_{CO} and the Weiss temperature Θ decrease linearly with increasing concentration y, which matches with the mean field theory. It was shown also that Fe is involved in AF exchange with the manganese. Iron-doped samples retain the superstructure for $T < T_{CO}$, but the q vector, the superstructure parameter, becomes depressed. In 5% Fe-doped samples the q vector was 12–15% smaller than that of the starting sample. This superstructure acquires an incommensurate character because of the appearance of defects in the formation of $Mn^{3+}O_6$ and $Mn^{4+}O_6$ stripes.

We report here on a study of the effect of copper doping on charge-orbital ordering in ceramic $La_{1/3}Ca_{2/3}Mn_{1-y}Cu_yO_3$ samples for $0 \le y \le 0.07$.

2. EXPERIMENTAL TECHNIQUE AND SAMPLE CHARACTERIZATION

Samples of undoped $La_{1/3}Ca_{2/3}MnO_3$ (LCMO) and of copper-doped $La_{1/3}Ca_{2/3}Mn_{1-y}Cu_yO_3$ ($0 \le y \le 0.07$) (LCMCuO) ceramic were obtained by standard solid-state reactions similar to the one employed earlier to prepare $La_{1-x}Ca_xMnO_3$ [19, 20]. La_2O_3 powder being hygroscopic, it was preliminarily annealed. Mixtures of the La_2O_3, $CaCO_3$, MnO_2, and CuO oxide powders were calcined in air at 1320°C for 40 h with intermittent grinding. The powder thus prepared was pelletized at a pressure of 2000 kg/cm^2 and calcined in air at 1370°C for 22 h.

The X-ray powder diffraction patterns (Fig. 1) showed all the samples to be single phase and have orthorhombic, *Pbnm*-type perovskite structure with lattice parameters $a \approx b \approx \sqrt{2}a_p$ and $c \approx 2a_p$ (where $a_p \sim$ 3.9 Å is the lattice parameter of basic perovskite [13]). Doping with copper to $0 \le y \le 0.07$ did not initiate formation of any secondary phases, and the lattice parameters remained practically unchanged.

The chemical composition was monitored on the local level in situ by energy dispersive X-ray analysis with a transmission scanning microscope on EDX samples ~1 nm in size. The chemical composition of both undoped LCMO and copper-doped LCMCuO samples was found to be uniform both within a grain and from one grain to another. In the LCMCuO samples, copper was distributed uniformly within a grain, with variation among grains being slightly larger. The average Cu content in grains was close to the required value of y.

We also performed a TEM study of 20 grain boundaries in Cu-doped samples by EDX. Copper was found to have segregated at all the boundaries studied. Figure 2 displays a typical Cu concentration profile along the direction perpendicular to the boundary plane. The concentration of Cu at the boundaries was 1.8–2.0 times that in the nearest grains separated by this boundary; Cu was observed to segregate only within a very narrow, ~1.5-nm thick, region on both sides of the boundary.

The oxygen content in the samples was checked by iodometric titration like this was done in [21]. The content of oxygen in undoped and copper-doped samples with low copper concentrations ($0 < y \le 0.01$) was very close to the nominal value of 3.0, whereas for heavy doping levels ($y \ge 0.04$) a certain oxygen deficiency was detected (see the table).

The behavior of the magnetization with temperature was studied with a SQUID magnetometer in the temperature range $T = 4.2$–400 K and in magnetic fields of up to 1 T. The sample was cooled from room temperature down to 4.2 K in zero field (ZFC regime) or in a constant field $B = 1$ T (FC regime).

The electrical resistivity measurements, $\rho(T)$, were carried out by the standard four-probe technique in heating and cooling runs.

The thermal properties of LCMO and LCMCuO were studied with a DSC-2 calorimeter (Perkin-Elmer) in nitrogen environment under varied heating and cooling rates. The temperature scale was calibrated against the melting points of ice (273.1 K) and indium (429.7 K), and the heat flow rate scale, against the white sapphire heat capacity. The samples chosen for the calorimetric measurements were ~50 mg in mass.

Possible formation of a superstructure as a result of charge and orbital ordering was studied by analyzing electron diffraction (ED) patterns and high-resolution electron-microscope images obtained at room temperature and 91 K with a TEM (Jeol 2010 F) operated at 200 kV and equipped by a field emission gun. The sample was fixed in a special holder cooled by liquid nitrogen, which permitted scanning in temperature and measurements at a fixed temperature in the 90–300-K range, as well as a two-coordinate change of sample tilt by ±15°. The samples intended for electron microscope studies were prepared by mechanical polishing to a thickness of 25–30 μm, followed by argon ion milling to a thickness transparent for electrons.

3. RESULTS AND DISCUSSION

Figure 3a plots the behavior with temperature of the magnetization M for the starting LCMO and the copper-doped LCMCuO samples measured in a magnetic field $H = 1$ T after preliminary cooling in zero magnetic field. The magnetization peak observed in the starting sample results from the sample transition to the charge-orbital ordering state and is well documented in literature [18, 22, 23]. The temperature T_{CO} at which this peak is observed is known as the charge ordering temperature. Doping with copper shifts the magnetization peak in $M(H)$ toward lower temperatures, with the peak amplitude decreasing markedly already at low copper concentrations $y = 0.005$ and 0.010. The variation of T_{CO} with copper concentration is shown graphically in Fig. 4a. Also shown for comparison is a $T_{CO}(y)$ graph obtained [18] for the case of iron doping of $La_{1/3}Ca_{2/3}Mn_{1-y}Fe_yO_3$ samples. We see that even low copper concentrations, $y \le 0.01$, bring about a substantial depression of T_{CO}, which demonstrates subsequently only a slight falloff as the copper concentration is increased still more. In the case of doping with trivalent iron Fe^{3+} the $T_{CO}(y)$ graph is found to be linear throughout the doping interval of $0 \le y \le 0.06$ [18].

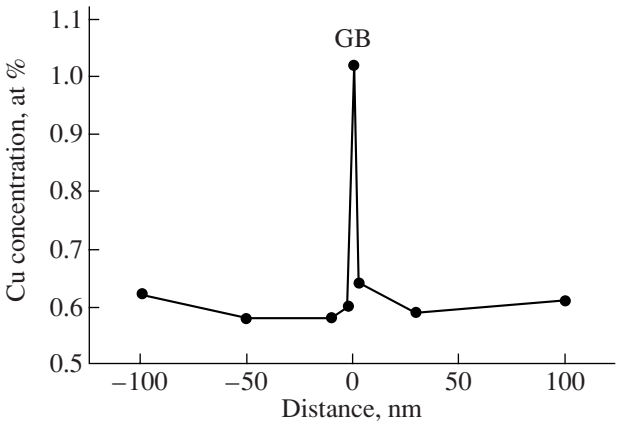

Fig. 2. Typical copper segregation profile obtained in measurements of the copper concentration across the grain boundary (GB) in $La_{1/3}Ca_{2/3}Mn_{1-y}Cu_yO_3$ ($y = 0.05$).

Note that the presence of copper does not initiate an increase in the FM component. In Fig. 3b, the temperature dependences of magnetization M drawn for some LCMCuO compositions are confronted with those obtained for the undoped LCMO composition in the ZFC and FC regimes in a magnetic field $H = 1$ T. In the undoped sample, the ZFC and FC magnetizations measured for $T < T_{CO}$ are observed to be irreversible, as this was reported in [18], where this feature was shown to originate from formation of small FM clusters, with the FM component being negligible (<0.3% of the FM saturation level in this system). Doping with copper depresses the irreversibility of magnetization still more.

Results of the iodometric titration of the $La_{1/3}Ca_{2/3}Mn_{1-y}Cu_yO_{3-\delta}$ samples ($0 \le y \le 0.07$)

Composition (y)	Oxygen content ($3 - \delta$)
0	2.980
0.01	2.975
0.04	2.965
0.07	2.950

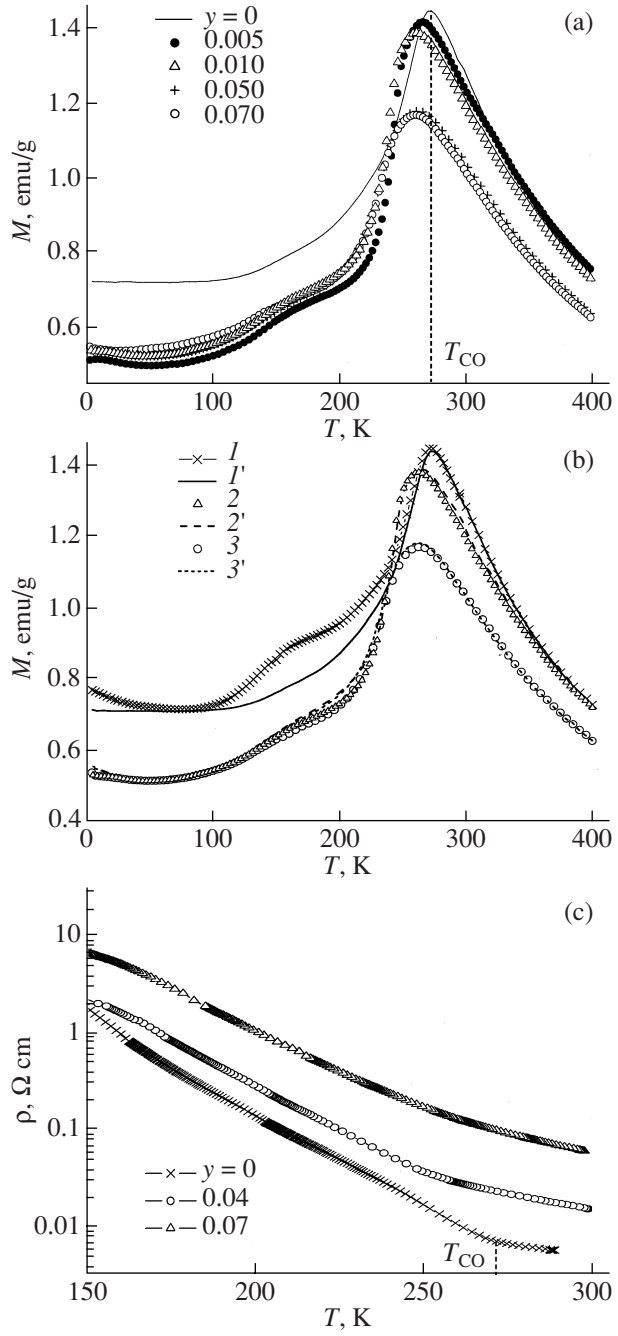

Fig. 3. (a) Temperature dependences of the magnetization of the copper-doped $La_{1/3}Ca_{2/3}Mn_{1-y}Cu_yO_3$ samples measured in a magnetic field of 1 T under ZFC conditions. (b) Temperature dependences of the magnetization of the copper-doped $La_{1/3}Ca_{2/3}Mn_{1-y}Cu_yO_3$ samples (y = (*1*, *1*') 0, (*2*, *2*') 0.01, and (*3*, *3*') 0.07) measured in a magnetic field of 1 T under (*1–3*) ZFC and (*1–3*) FC conditions. (c) Temperature dependences of the electrical resistivity of the copper-doped $La_{1/3}Ca_{2/3}Mn_{1-y}Cu_yO_3$ samples.

One sees both in the starting and the doped samples a certain hump in magnetization near 170 K, which is attributed in literature to AF ordering (in the starting sample the Néel temperature $T_N \approx 170$ K [23]).

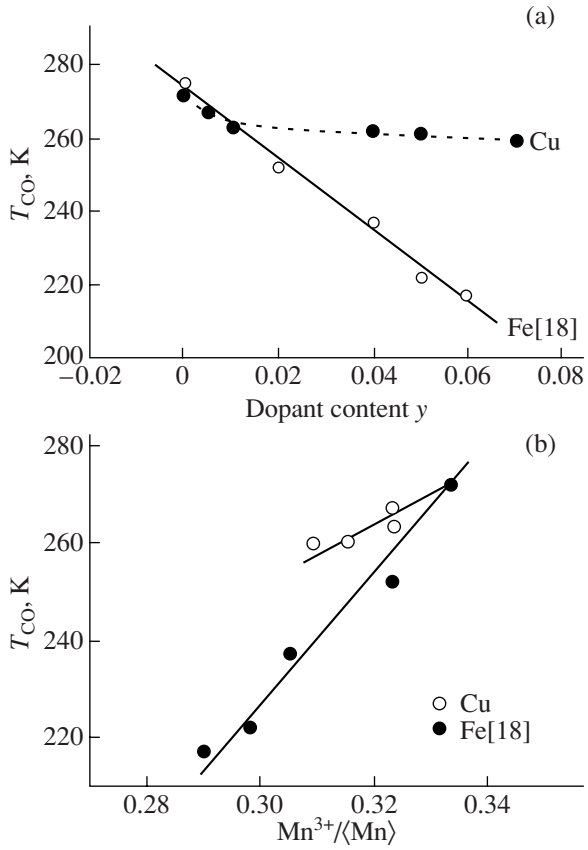

Fig. 4. Dependences of the charge ordering temperature T_{CO} on (a) the concentration y of dopant M in $La_{1/3}Ca_{2/3}Mn_{1-y}M_yO_3$ and (b) the concentration $n_{Mn^{3+}} = Mn^{3+}/\langle Mn\rangle$, where $\langle Mn\rangle = Mn^{3+} + Mn^{4+}$. M = Cu (this work) and Fe [18].

The temperature dependences of the electrical resistivity ρ were measured for all LCMCuO samples with copper concentrations $0 \le y \le 0.07$. Figure 3c presents only a part of these graphs, with the rest being dropped not to overload the figure. The semiconducting character of the $\rho(T)$ plots is retained for all the copper-doped compounds, and the electrical resistivity varies very little throughout the doping interval of $0 \le y \le 0.07$. As the temperature is lowered, one observes, starting from T_{CO} (the inherent temperature for each compound), a faster growth of the electrical resistivity, which can be assigned to a change in the conditions of charge transfer between the Mn^{3+} and Mn^{4+} ions initiated by charge ordering [24]. The values of T_{CO} derived from measurements of the temperature dependences of magnetization fit well the value at which the resistivity starts to rise more steeply.

Thus, throughout the copper doping region studied the physical relations $\rho(T)$ and $M(T)$ exhibit a pattern characteristic of the transition to the charge ordering state.

Because, as already mentioned, the relative concentrations of the Mn^{3+} and Mn^{4+} ions play an essential part in manifestation of the various manganite properties, one has to start with estimating the fraction of Mn^{3+} ions in the copper-doped samples. Choosing fixed valences for La (3+), Ca (2+), and Cu (2+) (the choice of the 2+ valence state for copper will be discussed later on), as well as taking into account the iodometric titration data (the oxygen content) and assuming charge balance, we can determine the concentration of Mn^{3+} ions $n_{Mn^{3+}} = Mn^{3+}/(Mn^{3+} + Mn^{4+})$ for the copper-doped samples. It turned out that $n_{Mn^{3+}}$ varied within a narrow interval of 0.333–0.310 with y varied from 0 to 0.07. The explanation for such a small variation of the Mn^{3+} concentration lies in that at heavy doping levels ($y \geq 0.04$) replacement of Mn^{3+} by divalent copper Cu^{2+} brought about an oxygen deficiency (see table). The $T_{CO}(n_{Mn^{3+}})$ relations reduced for the case of copper doping are confronted in Fig. 4b with those obtained for doping with iron [18]. We readily see that in the case of copper doping the $T_{CO}(n_{Mn^{3+}})$ relation approximates a linear plot too; said otherwise, the Mn^{3+} ion concentration is a major factor governing the value of T_{CO}. The Mn^{3+} concentrations obtained for the copper-doped samples lie within the region which is characterized by charge ordering accompanied by formation for $T < T_{CO}$ of long-range order superstructures in the case of doping by other elements, for instance, by iron [18].

The effect of copper doping on charge ordering at the structural level was studied with an electron microscope by analyzing ED patterns and HREM images at 91 and 300 K. We note that selective electron diffraction was measured primarily from the (00l) basal planes within a selected area of a crystallite, where one studied both different regions within a separate grain and different grains. One compared ED patterns obtained at room temperature and at 91 K. The ED patterns obtained from an undoped sample at 91 K contained additional satellite reflections with $q = 1/3a^*$ (a^* is the reciprocal lattice vector), a feature typical of the formation of a superstructure with a triple lattice parameter $3a$. The HREM images provided supportive evidence for the existence of such a commensurate superstructure with the $3a$ parameter. These electron microscope observations obtained for an undoped compound are similar to those reported earlier [18] in a detailed study of both ED and HREM images for the starting undoped compound $La_{1/3}Ca_{2/3}MnO_3$.

Similar electron microscope studies performed on copper-doped samples, including samples with a low Cu concentration $y = 0.01$, did not reveal any indication of superstructure formation. The ED patterns obtained at 91 K did not contain any additional reflections. These ED patterns did not differ in anything from those measured at room temperature. Figure 5a displays the diffraction pattern obtained at 91 K for a copper-doped sample ($y = 0.02$) and demonstrating the absence of any additional reflections besides the main Bragg peaks (which correspond to the orthorhombic *Pbnm* structure). Figure 5b presents the HREM image corresponding to this ED pattern.

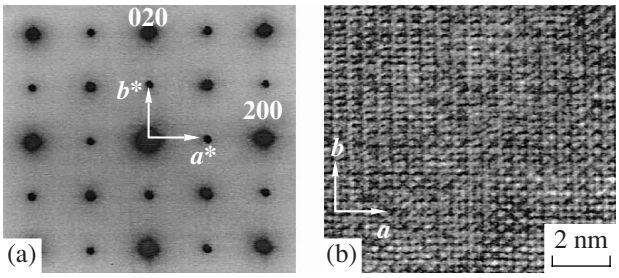

Fig. 5. (a) Electron diffraction pattern and (b) the corresponding high-resolution electron microscope image obtained at a temperature of 91 K from the zone with the [001] normal in the $La_{1/3}Ca_{2/3}Mn_{1-y}Cu_yO_3$ ($y = 0.02$) samples.

Thus, in the case of copper doping a careful TEM study of a large number of grains (crystallites) did not detect any signs of formation of a superstructure, in either direct electron images or in the diffraction patterns. At the same time, the physical characteristics $\rho(T)$ and $M(T)$ follow a pattern suggesting transition to the CO state. It appears only natural to assume that we deal here with a kind of charge ordering which does not have long-range order but follows instead a certain short-range order, a situation that could account for the observed behavior of the physical properties $\rho(T)$ and $M(T)$ while not favoring formation of a regular superstructure with long-range order. It should be stressed that copper introduced in as low a concentration as $y = 0.01$ suppresses formation of a superstructure with long-range order.

Because 3+ is an extremely rare valence state for copper [25], our analysis of the results of this experiment performed as this was done in [25] assumed the 2+ valence in $La_{1/3}Ca_{2/3}Mn_{1-y}Cu_yO_3$. The case of substitution of the manganese ion with divalent copper differs substantially from Mn replacement with trivalent ions, for instance, with Fe^{3+}. To start with, Cu^{2+} has a noticeably larger ionic radius. In the case of doping with the divalent copper ion the difference in size between the Cu^{2+} and Mn^{3+} ions is $(r_{Mn^{3+}} - r_{Cu^{2+}}) = -0.06$ (~9%), or >16% compared with the average manganese ion $\langle Mn \rangle$ size in the compound. In the case of iron doping (Fe^{3+}), this difference is of the opposite sign and substantially smaller in magnitude, $(r_{Mn^{3+}} - r_{Fe^{3+}}) = 0.02$. The markedly larger Cu^{2+} ion inserted in place of Mn^{3+} is capable of generating an internal pressure and initiating, apparently, a local change of the lattice parameters, although, as mentioned above, the lattice parameters derived from X-ray diffraction analysis of undoped and copper-

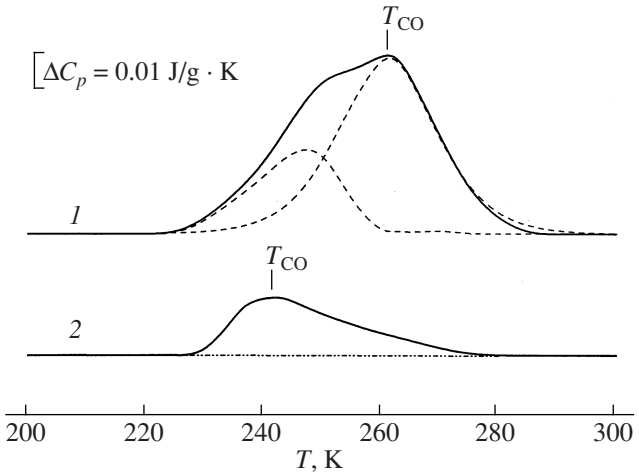

Fig. 6. DSC curves (solid lines) obtained during heating of (*1*) $La_{1/3}Ca_{2/3}MnO_3$ and (*2*) $La_{1/3}Ca_{2/3}Mn_{1-y}Cu_yO_3$ samples for $y = 0.04$. The dashed line indicates the decomposition of the peak for the $La_{1/3}Ca_{2/3}MnO_3$ sample into two constituents (see text). The scanning rate is $v = 1.25$ K min^{-1}.

doped samples practically do not differ. Second, there is a possibility that the presence of a divalent ion which cannot transfer to a higher valence state may increase the time the Mn ions can reside in a higher valence state, i.e., as Mn^{4+} in the nearest environment of the Cu^{2+} ion. Because Mn^{4+} has a smaller ionic radius than Mn^{3+}, the assumed local charge "ordering" should bring about straightening of the nearest Mn^{3+}–O–Mn^{4+} bonds, thus relieving the strains in the system (by acting accordingly on the Jahn–Teller distortion of the $Mn^{3+}O_6$ octahedra in the nearest environment). All this should certainly interfere with long-range charge and orbital ordering. At high copper concentrations ($y \geq 0.04$), the presence of oxygen vacancies should additionally increase disorder in the Mn^{3+}–O–Mn^{4+} bond system.

It is worthwhile to note that substitution of univalent copper (Cu^+) for Mn^{3+}, a case not considered here, would strengthen still more the factors tending to depress long-range order in charge ordering, because the differences both in the ionic radii and in charge between the Cu^+ and Mn^{3+} ions are still larger.

An indirect support for our assumption that copper doping brings about charge ordering with a much poorer degree of order comes from differential scanning calorimetry measurements (DSC). Figure 6 presents DSC curves obtained under heating of $La_{1/3}Ca_{2/3}MnO_3$ and $La_{1/3}Ca_{2/3}Mn_{1-y}Cu_yO_3$ ($y = 0.04$) crystals. We readily see that doping with copper brings about strong suppression of the thermal effect of the phase transition caused by charge ordering [26–28] and a decrease in the transition enthalpy (ΔH) from 1.79 to 0.44 J/g and of the transition entropy (ΔS) from 0.007 to 0.002 J/g K. Reduced to an integer number of atoms in the crystal, the above values of the entropy become 0.88 and 0.25 cal/mol K. The transition temperature T_{CO} is also lowered by doping. The shape of the peak in the DSC curve for the undoped sample suggests the presence of at least two components. This is argued for also by data on Bragg scattering in samples of the same composition which are reported in [26].

The phase transition occurring under charge ordering in $La_{1/3}Ca_{2/3}MnO_3$ is a two-component transformation (Fig. 6, dashed lines under curve *1*). It turned out that it is close in physical nature to a second-order phase transition of the order–disorder type. The entropy of such a transition is known to be ~1 cal/mol K [29], a figure comparable in magnitude with $\Delta S = 0.88$ cal/mol K obtained in this study. This suggests that the decrease in the transition entropy observed in the doped sample can be safely attributed to the decrease in the degree of order in the regular superstructure characteristic of the undoped starting compound.

To sum up, we have studied the effect of doping with copper on charge ordering in $La_{1/3}Ca_{2/3}Mn_{1-y}Cu_yO_3$ ($0 \leq y \leq 0.07$). It has been shown that copper becomes uniformly distributed over manganese lattice sites and segregates additionally at grain boundaries within a narrow region of $\leq \pm 1.5$ nm.

Doping with copper gives rise to a depression of the charge ordering temperature T_{CO}, with $T_{CO} \sim n_{Mn^{3+}}$. Doping with copper does not affect the pattern of behavior of $M(T)$ and $\rho(T)$; at the same time, even low copper concentrations ($y = 0.01$) suppress completely the formation of the CO/OO long-range order superstructure typical of the $La_{1/3}Ca_{2/3}MnO_3$ undoped compound. It is assumed that replacement of trivalent manganese with divalent copper, which has both a smaller charge and a larger ionic radius, gives rise to larger local distortions of the Mn^{3+}–O–Mn^{4+} bonds, strong enough to disrupt the CO/OO long-range order. Our calorimetric measurements reveal that the transition to CO at T_{CO} in copper-doped samples is indeed accompanied by a substantially smaller change in the entropy factor compared with the case of the undoped compound.

ACKNOWLEDGMENTS

We are grateful to G. Vetter for assistance in performing X-ray diffraction measurements.

REFERENCES

1. *Colossal Magnetoresistance Oxides*, Ed. by Y. Tokura (Gordon and Breach, New York, 2000).
2. J. Cocy, M. Viret, and S. Molnar, Adv. Phys. **48**, 167 (1999).
3. M. B. Salamon and M. Jaime, Rev. Mod. Phys. **73**, 583 (2001).
4. Yu. A. Izyumov and Yu. N. Skryabin, Usp. Fiz. Nauk **171** (2), 121 (2001) [Phys.—Usp. **44** (2), 109 (2001)].

5. V. M. Loktev and Yu. G. Pogorelov, Fiz. Nizk. Temp. (Kharkov) **26** (3), 231 (2000) [Low Temp. Phys. **26** (3), 171 (2000)].
6. E. Dagotto, H. Hotta, and A. Moreo, Phys. Rep. **344**, 1 (2001).
7. E. L. Nagaev, *Colossal Magnetoresistance and Phase Separation in Magnetic Semiconductors* (Imperial College Press, London, 2002).
8. C. Zener, Phys. Rev. **82**, 403 (1951).
9. J. P. Goodenough, Phys. Rev. **100**, 564 (1955).
10. G. C. Milward, M. J. Calderon, and P. B. Littlewood, Nature (London) **433**, 607 (2005).
11. M. Coey, Nature (London) **430**, 154 (2004).
12. C. H. Chen and S.-W. Cheong, Phys. Rev. Lett. **76**, 4042 (1996).
13. C. H. Chen, S.-W. Cheong, and H. Y. Hwang, J. Appl. Phys. **81**, 1326 (1997).
14. J. Herrero-Martin, J. Garcia, G. Subias, J. Blasco, and M. Concepcion Sánchez, Phys. Rev. B: Condens. Matter **70**, 024408-1 (2004).
15. J. Garcia, M. Concepcion Sánchez, J. Blasco, G. Subias, and M. Grazia Proietti, J. Phys.: Condens. Matter **13**, 3243 (2001).
16. G. van Tendeloo, O. I. Lebedev, M. Herview, and B. Raveau, Rep. Prog. Phys. **67**, 1315 (2004).
17. Y. Jo, J.-G. Park, C. S. Hong, N. H. Hur, and H. C. Ri, Phys. Rev. B: Condens. Matter **63**, 172413 (2001).
18. T. S. Orlova, J. Y. Laval, P. Monod, J. G. Noudem, V. S. Zahvalinskii, V. S. Vikhnin, and Yu. P. Stepanov, J. Phys.: Condens. Matter **18**, 6729 (2006).
19. R. Laiho, K. G. Lisunov, E. Lähderanta, P. A. Petrenko, J. Salminen, V. N. Stamov, and V. S. Zakhvalinskii, J. Phys.: Condens. Matter **12**, 5751 (2000).
20. R. Laiho, K. G. Lisunov, E. Lähderanta, P. A. Petrenko, V. N. Stamov, and V. S. Zakhvalinskii, J. Magn. Magn. Mater. **213**, 271 (2000).
21. M. C. Wu, J. Chen, and X. Jin, Physica C (Amsterdam) **276**, 132 (1997).
22. P. G. Radeaelli, D. E. Cox, L. Capogna, S.-W. Cheong, and M. Marezio, Phys. Rev. B: Condens. Matter **59**, 14440 (1999).
23. T. Sudyoadsuk, R. Suryanarayanan, P. Winotai, and L. E. Wenger, J. Magn. Magn. Mater. **278**, 96 (2004).
24. M. R. Ibarra, J. M. de Teresa, J. Blasco, P. A. Algarabel, C. Marquina, J. Garcia, J. Stankiewicz, and C. Ritter, Phys. Rev. B: Condens. Matter **56**, 8252 (1997).
25. S. B. Ogale, R. Shreekala, R. Bathe, S. K. Date, S. I. Patil, B. Hannoyer, F. Petit, and G. Marest, Phys. Rev. B: Condens. Matter **57**, 7841 (1998).
26. A. P. Ramirez, P. Schiffer, S.-W. Cheong, C. H. Chen, W. Bao, T. T. M. Plasta, P. L. Gammel, D. J. Bishop, and B. Zegarski, Phys. Rev. Lett. **76**, 3188 (1996).
27. A. P. Ramirez, S.-W. Cheong, and P. Schiffer, J. Appl. Phys. **81**, 5337 (1997).
28. M. T. Fernandez-Diaz, J. L. Martinez, J. M. Alonso, and E. Herrero, Phys. Rev. B: Condens. Matter **59**, 1277 (1999).
29. B. A. Strukov and A. P. Levanyuk, *Ferroelectric Phenomena in Crystals: Physical Foundations* (Nauka, Moscow, 1983; Springer, Berlin, 1998).

Translated by G. Skrebtsov